



Product characteristics and heat of reaction of municipal solid waste in pyrolysis and gasification at low temperatures

Yuya Sakurai¹ · Eriko Sugimura² · Tsutomu Ito² · Hiroki Harada²

Received: 2 August 2023 / Accepted: 17 January 2024 / Published online: 2 March 2024
© The Author(s), under exclusive licence to Springer Nature Japan KK, part of Springer Nature 2024

Abstract

This study examines the pyrolysis and gasification characteristics of municipal solid waste (MSW) via thermogravimetric analysis and laboratory-scale pyrolysis and gasification experiments. The MSW samples were directly collected from an operational MSW incineration plant in Japan. The MSW was classified into 10 visually distinguishable components, which were further categorized as biomass and plastics. The thermogravimetric analysis of each MSW component of the experimental samples demonstrated distinct weight loss patterns between biomass and plastics but similarities within their respective categories. Subsequently, laboratory-scale pyrolysis and gasification experiments were conducted in a $N_2 + H_2O$ atmosphere at heating temperatures of 450, 550, and 650 °C. The steam-to-carbon ratio (S/C) was set to 2.0. Char, coke, wax, tar, and gas were identified as pyrolysis gasification products, with the major components of tar and gas being determined. The experimental findings revealed the pyrolysis and gasification product yields of biomass and plastics that make up the refuse within a temperature range of 450 to 650 °C. Moreover, the heat of reaction for pyrolysis and gasification ranged from -661 to -237 J/g–sample (db) (exothermic reaction) for biomass and 4649 to 8106 J/g–sample (db) (endothermic reaction) for plastics.

Keywords Municipal solid waste · Pyrolysis · Gasification · Tar · Heat of reaction

Introduction

Growing concerns regarding the various environmental crises precipitated by global warming have propelled worldwide efforts to establish a carbon-neutral society in line with the objectives outlined in the Paris Agreement. The 6th Strategic Energy Plan (2021) in Japan explicitly emphasizes the imperative of transitioning to renewable energy as the primary power source to promote decarbonization, especially in the energy sector, which is a remarkable contributor to CO_2 emissions [1].

To advance decarbonization, Japan's waste and resource recycling sector must curtail general waste emissions by

minimizing incineration and landfill practices, introducing highly efficient energy recovery techniques, and implementing carbon capture, utilization, and storage technologies for general waste. Moreover, Japan is aiming for a transition to a regionally decentralized society, which is driven by factors such as population decline and the need to address large-scale weather disasters [2]. Waste treatment facilities also play an important role in fostering sustainable and resilient urban development. These facilities hold promise as regional energy and disaster prevention centers. Consequently, irrespective of their scale, the development of systems capable of attaining high energy recovery efficiency assumes paramount importance for waste treatment facilities. Currently, MSW power generation relies on the use of heat from waste combustion as electrical energy through the MSW incineration plant's boilers, steam turbines, and generators (BTG). However, BTG power generation typically requires large facilities for efficient electricity production. Therefore, numerous small- to medium-scale facilities, especially those with a throughput of less than 100 tons/day, encounter challenges associated with low power generation efficiency and insufficient energy recovery [3, 4].

✉ Yuya Sakurai
sakurai.y@hitachizosen.co.jp

¹ Technical Research Institute, R&D Headquarters, Hitachi Zosen Corporation, 2-11, Funamachi 2-Chome, Taisho-Ku, Osaka 551-0022, Japan

² Business & Product Development Division (Center), Hitachi Zosen Corporation, 7-89, Nankokita 1-Chome, Suminoe-Ku, Osaka 559-8559, Japan

In recent years, the utilization of pyrolysis and gasification has emerged as a highly efficient approach for energy recovery from MSW, even in treatment facilities with small to medium volumes [5]. Pyrolysis and gasification are prominent techniques within the realm of thermochemical conversion employed for the conversion of solid organic resources, such as coal and woody biomass, into gaseous fuels. This technology involves subjecting organic materials to elevated temperatures in an O₂-free or low-O₂ atmosphere, leading to the disintegration of molecular chains in solid polymers through pyrolytic reactions. Consequently, this process yields low-molecular-weight gases, notably synthesis gases comprising hydrogen (H₂) and carbon monoxide (CO). Simultaneously, the deliberate introduction of oxidizers, such as H₂O or CO₂, is commonly used to promote gasification and reforming reactions of carbon present in solid and liquid phases, augmenting the gas output in the product [6, 7]. The generated gas holds potential as a gaseous fuel for gas engines, fuel cells, gas turbines, and other applications. Considerably more efficient than conventional BTG power generation in small- and medium-scale power generation facilities, pyrolysis and gasification methods are anticipated to offer sufficient efficiency even when handling smaller MSW volumes [8, 9].

Various types of pyrolysis and gasifiers have been extensively studied for the processing of MSW, including fixed bed gasifiers [10–13], bubbling and circulating fluidized bed gasifiers [14, 15], and rotary kiln gasifiers [16–18]. Among these options, the rotary kiln gasifier has gained substantial popularity due to its ability to effectively handle feedstocks with diverse compositions, superior tolerance for high moisture content in refuse, uniform heating of refuse facilitated by the rotary motion of the gasifier, and flexibility in pyrolysis conditions [19, 20]. When using a rotary kiln gasifier for MSW gasification, an indirect heating method utilizing char combustion heat is commonly employed to ensure the production of high-quality gas with a high calorific value. The temperature range near the feed inlet of the rotary kiln gasifier, which is externally heated, typically falls within 400 to 600 °C, promoting initial pyrolysis of the MSW within this range. Subsequently, in the middle and near the outlet of the rotary kiln gasifier, temperatures ranging from 700 to 900 °C foster gasification and reforming reactions of char and tar as secondary processes to pyrolysis products [21]. Given the sequential and parallel nature of these reactions inside the rotary kiln gasifier, distinguishing between the initial pyrolysis, gasification, and reforming reactions becomes challenging. Therefore, it is pertinent to comprehend the reaction characteristics of refuse across various temperature ranges to design an optimal rotary kiln gasifier. Notably, the mass and heat balance during the

initial pyrolysis significantly influence the final pyrolysis gasification product composition [22] and play a crucial role in determining the temperature control index in the pyrolysis zone of the rotary kiln gasifier.

Previous studies have examined the pyrolysis and gasification characteristics of MSW through various investigations. Fundamental investigations have been conducted using simulated MSW samples (pure paper and plastic) to explore the material balance in the pyrolysis and gasification processes [23, 24]. However, studies employing MSW samples collected directly from treatment facilities, which inherently represent complex multi-component mixtures, are currently insufficient [25]. Furthermore, in the design of gasifiers, it is crucial to evaluate the products resulting from pyrolysis and gasification from a thermal perspective and elucidate the heat balance within the pyrolysis and gasification reaction processes. Generally, the reaction heat of the pyrolysis process is measured using differential scanning calorimetry (DSC) [26–28]. Nonetheless, considering that the pyrolysis gasification reaction process is remarkably affected by gas-phase reactions and is highly dependent on equipment and reaction conditions, a direct estimation from pyrolysis gasification products in a laboratory-scale or larger experimental environment becomes necessary.

This study aimed to conduct laboratory-scale experiments to evaluate the pyrolysis and gasification characteristics of MSW within the temperature range 450 to 650 °C, corresponding to the vicinity of the feedstock inlet of a rotary kiln gasifier, focusing on mass balance and heat balance. The experimental samples were collected from an operational MSW incineration plant in Japan. Usually, because of regional and seasonal variations in the composition of MSW, it is necessary to separate it into components with similar physical and chemical characteristics. Once the pyrolysis and gasification characteristics of each classification category are clarified, it will be possible to predict reactions for MSW with different compositions. The MSW samples were classified into two main categories based on similarities in pyrolysis characteristics: biomass and plastics. The biomass group comprised paper (PA), cloth (CL), wood, bamboo, straw (WBS), kitchen waste (KW), and dirty paper (DP). The plastics group consisted of vinyl and plastic and synthetic resins (SR). Thermogravimetric analysis was performed to generate thermogravimetric curves for the experimental samples. Subsequently, laboratory-scale pyrolysis and gasification experiments were conducted at temperatures of 450, 550, and 650 °C. The main pyrolysis gasification products at each heating temperature were collected, and the mass balance was evaluated. After measuring the higher heating values (HHV) of the products, the heat balance was calculated from the higher heating values of the MSW and products to obtain the reaction heat in the pyrolysis and gasification reactions.

Materials and methods

MSW samples

Experimental samples were collected from a Japanese MSW incineration plant. The MSW was classified into 10 visually distinguishable categories [30], following the guidelines outlined in Japan's Kansei No. 95 [29]. Table 1 provides detailed information on the MSW classification items and their respective abundance ratios at the time of collection. Based on previous studies [31, 32], the pyrolysis characteristics of the components within biomass and plastics were found to be similar, with limited interactions among components within the same category. Hence, for this study, the MSW samples were divided into biomass and plastics as the experimental samples. Three types of materials were excluded from this study: incombustibles, which are challenging to identify and reproduce as non-organic materials; others; and plastic bottles, which were not contaminated in this sampling.

Table 2 presents the results of the proximate analyses, ultimate analyses, calorific values, and mixing ratios of the experimental samples. The experimental samples were ground into a powder with a particle size < 0.1 mm. Notably, vinyl proved difficult to grind into a powder, resulting in some vinyl particles with a diameter as small as 1 mm. To ensure a representative composition, the experimental samples were mixed and processed for each experiment. The mixing ratios (Table 2) were determined to match the proportions of biomass and plastics present in the MSW samples (Table 1) at the time of collection. Subsequently, the mixed experimental samples were packed into alumina boats with a predetermined weight of 4.0 ± 0.01 g

and subjected to a drying treatment at a temperature of 105 °C for at least 12 h.

Thermogravimetric analysis

Thermogravimetric and differential thermal analysis (TG/DTA7200, Hitachi High-Tech Science Co.) was performed for each MSW component. An analytical sample was filled in a Pt container with 10 mg, while Al_2O_3 served as the reference material. N_2 was used as the carrier gas at a flow rate of 200 NmL/min. The temperature program involved a gradual increase of 10 °C/min, starting from 20 °C and reaching 110 °C, with a holding time of 1 h to establish the weight change based on the dry weight. Subsequently, the temperature was further increased from 110 to 1000 °C at a rate of 10 °C/min.

Laboratory-scale pyrolysis and gasification experiments

Experimental procedures

Figure 1 illustrates the experimental setup employed for the pyrolysis and gasification experiments. An alumina boat containing the experimental samples was placed in a quartz reaction tube (outer diameter: $\Phi 55$ mm; inner diameter: $\Phi 50$ mm; length: 850 mm). An alumina boat was positioned within a preheated Sect. (200 °C) covered with a mantle heater. In a horizontal electric furnace (350 mm), the center of the quartz reaction tube was heated to predetermined temperatures (450, 550, and 650 °C). The flow rates of the carrier gas, N_2 , and steam were controlled using a mass flow controller and a syringe pump, respectively, and introduced into the reaction tube. The heated section was defined as the

Table 1 Classification of MSW and the composition of the experimental samples used in this study

Classification in this study	Composition of MSW ¹	Representative example	Abundance ratio [wt% (db ²)]
Biomass	Paper (PA)	Newspapers, Magazines, and Cardboard	47.3
	Cloth (CL)	Clothing, Textile leather goods, and Sandals	8.52
	Wood, Bamboo, Straw (WBS)	Branches, Split branches, Grasses, Flowers, and Bamboo	10.4
	Kitchen waste (KW)	Food waste, Animal residues, and Eggshells	8.87
	Dirty paper (DP)	Diapers, Sanitary products	6.56
Plastic	Vinyl, Plastic containers (VP)	Garbage bags, and Styrofoam	12.7
	Synthetic resins (SR)	Plastic products, Rubber	0.88
Not used	Incombustible	Metals, Earth, Sand, Stones, and Glass	2.35
	Others	Passed through a 5-mm sieve	2.41
	PET bottle	PET bottle	0.00

¹Based on Kansei No. 95 [29];

²db: dry base

Table 2 Proximate analysis, ultimate analysis, calorific value, and mixing ratio in experimental samples

	Biomass					Plastic	
	PA	CL	WBS	KW	DP	VP	SR
Proximate analysis [wt% (wb ¹)]							
Moisture	44.9	24.2	48.7	72.7	69.9	15.9	5.50
Ash	5.84	1.90	3.03	3.03	3.22	2.02	6.24
Volatile matter	42.1	65.5	38.5	20.5	23.6	81.9	85.5
Fixed carbon	7.16	8.41	9.80	3.74	3.28	0.17	2.74
Ultimate analysis [wt% (db ²)]							
C	42.6	55.8	47.3	46.8	49.2	83.2	76.9
H	6.30	7.50	6.20	6.30	7.30	13.3	11.1
N	0.12	3.38	1.04	3.37	0.55	0.10	0.51
O ³	39.9	30.1	39.1	31.6	31.5	0.74	4.62
S	0.04	0.05	0.08	0.17	0.06	0.04	0.02
Cl	0.45	0.71	0.37	0.67	0.70	0.22	0.25
Calorific value [kJ/kg (db ²)]							
HHV	16,590	22,500	18,320	17,080	19,540	42,500	34,220
LHV	15,215	20,863	16,967	15,705	17,947	39,598	31,798
Mixing ratio [wt% (db ²)]							
Mixing ratio	57.9	10.4	12.8	10.9	8.03	93.6	6.44

¹wb, wet base
²db, dry base
³Calculated value

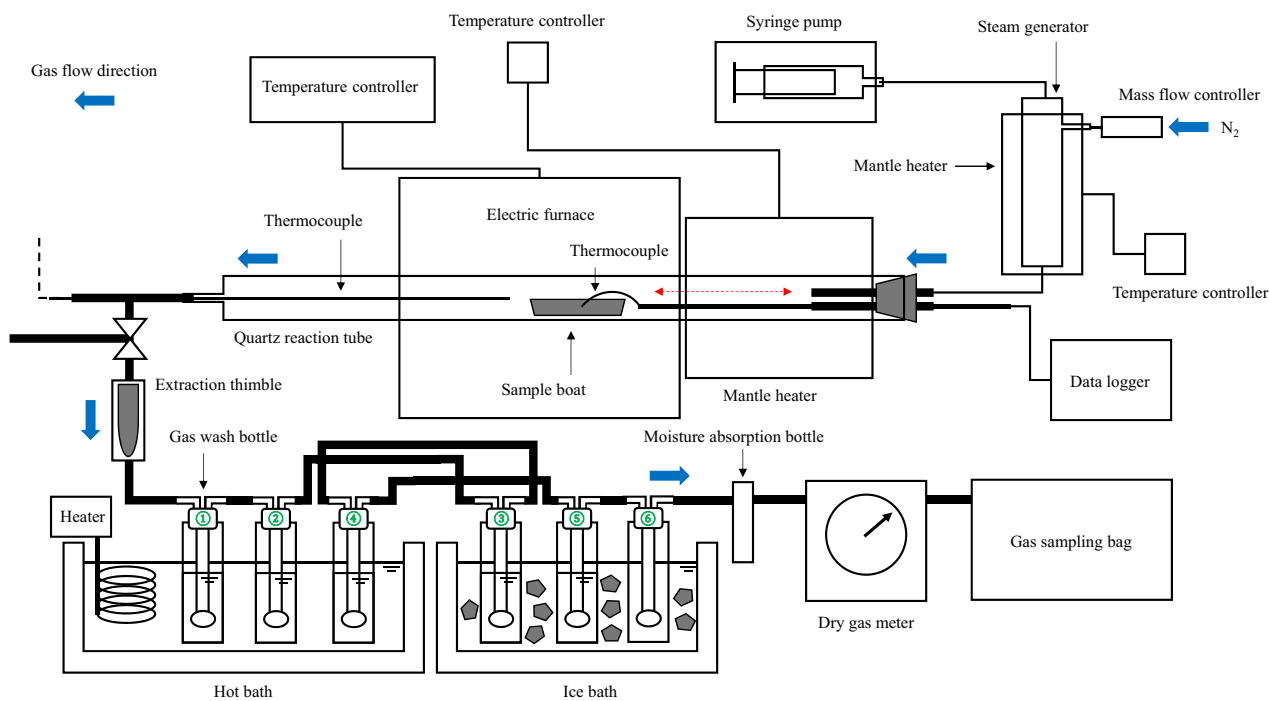


Fig. 1 Experimental device

region within $\pm 10\text{ }^\circ\text{C}$ of the designated heating temperature. The flow rates of N₂ and steam were adjusted to achieve a gas residence time of approximately 5 s within the heated

section. When using MSW as a gasification feedstock, the abundant moisture content of MSW must be taken into account. However, it is difficult to define a single value for

the moisture content of an irregular MSW. In this study, the steam-to-carbon ratio (*S/C*) was set to 2.0 to ensure relatively abundant steam in consideration of actual gasification process conditions. *S/C* was defined as the molar ratio of the amount of steam input to the amount of carbon in the experimental sample. Once the electric furnace reached the predetermined temperature, the experimental samples were moved from the preheating section to the heating section inside the electric furnace using a sliding method. Subsequently, the experimental samples were kept in the heated section for 20 min following the onset of heating.

The volatile components, encompassing tar and gas resulting from the pyrolysis and gasification of MSW, were passed through a sampling line maintained at 200 °C, which included an extraction thimble, with the tar collected in a gas cleaning bottle. In this study, the tar traps were constructed based on the tar guidelines/protocols (CEN/TS15439) established by the European Committee for Standardization (ECN) [33]. Specific details regarding the tar trap configuration are shown in Table 3. To clarify the location of the gas collection bottles, Figure 1 shows the gas collection bottle numbers corresponding to Table 3. The gas that passed through the tar trap underwent moisture removal in a moisture-absorbing bottle (containing CaCl₂ and glass wool). The total flow rate was measured using a dry gas meter, and all the gas was collected in a gas sampling bag.

Product analysis

Solid products derived from biomass include char and coke. Char and wax were identified as solid products originating from plastics. Pyrolysis and gasification of plastics at 450 °C was considered unreacted material rather than char, since the reaction was clearly not completed. Char represented the residue found on the alumina boat following pyrolysis and gasification. The solids collected on the outside of the alumina boat, such as on the wall of the quartz reaction tube or on the extraction thimble, were defined as coke (biomass) or wax (plastic), because they were generated as solids after some of the volatiles had aggregated in the gas phase [34].

Table 3 Configuration of the tar trap

No	Types of gas cleaning bottles	Capacity [mL]	Temp. [°C]	Solvent	Solvent quantity [mL]
1	Muenck type	250	40	IPA	50
2	G3	250	40	IPA	50
3	G3	250	−10	IPA	50
4	Muenck type	250	40	IPA	50
5	Muenck type	250	−10	IPA	50
6	Muenck type	250	−10	Empty	–

These products were determined through filtration of the washing solution from the quartz reaction tube and sampling line, which had been washed with acetone, as well as the Soxhlet-extracted solution (50 °C) on the extraction thimble. Any coke and wax that could not be removed via washing were considered losses. For analysis, the solids that were available in sufficient quantities underwent ultimate analysis and measurement of their higher heating values (HHV) according to JIS M 8814 [35].

The tar was a mixture of (1) the washing liquid obtained from cleaning the quartz reaction tubes and sampling lines with acetone; (2) the liquid collected with isopropyl alcohol (IPA) in a tar trap; and (3) the extracted liquid from Soxhlet extraction of the extraction thimble. The extraction thimble was dried at 80 °C for 3 h to remove water and then subjected to Soxhlet extraction for 16 h using acetone as the solvent. The Soxhlet extract from the extraction thimble was mixed with the other recovered tar solutions and subjected to crude concentration in an evaporator at 50 °C. Treatment with the evaporator was performed until no water droplets were observed on the glass surface of the flask. The coarsely concentrated tar was further heated on a hot plate at 80 °C to remove residual moisture, IPA, and acetone. Concentration was completed when the rate of tar weight loss was less than 0.05 wt%/h as a constant volume criterion. After the tar was concentrated, the tar weight was determined, followed by ultimate analysis and measurement of the HHV (JIS M 8814 [35]). For certain conditions, the concentrated tar obtained during the concentration process was used for qualitative analysis of its components using gas chromatography–mass spectrometry (GC–MS, 6890/5973N, Agilent Technologies).

The gas collected in the gas sampling bag underwent qualitative quantification of representative components using a gas chromatograph (GC). H₂, O₂, N₂, CH₄, CO, and CO₂ were analyzed via GC-TCD (GC7100TF, J-Science Lab Co., Ltd.), using Ar as the carrier gas. C₂H₂, C₂H₄, C₃H₆, C₃H₈, n-C₄H₁₀, and iso-C₄H₁₀ were analyzed via GC-FID (GC7100TF, J-Science Lab Co., Ltd.) using He as the carrier gas.

Results and discussion

Thermogravimetric analysis of MSW components

The thermogravimetric curves and thermogravimetric derivative curves for biomass and plastics are shown in Figs. 2 and 3, respectively, illustrating the fundamental pyrolysis characteristics of the seven MSW components investigated in this study. Figure 2 reveals that the main pyrolysis temperatures are similar for the same category of biomass. The same trend was observed for plastics (Fig. 3). These findings validate the approach adopted in this study, wherein MSW

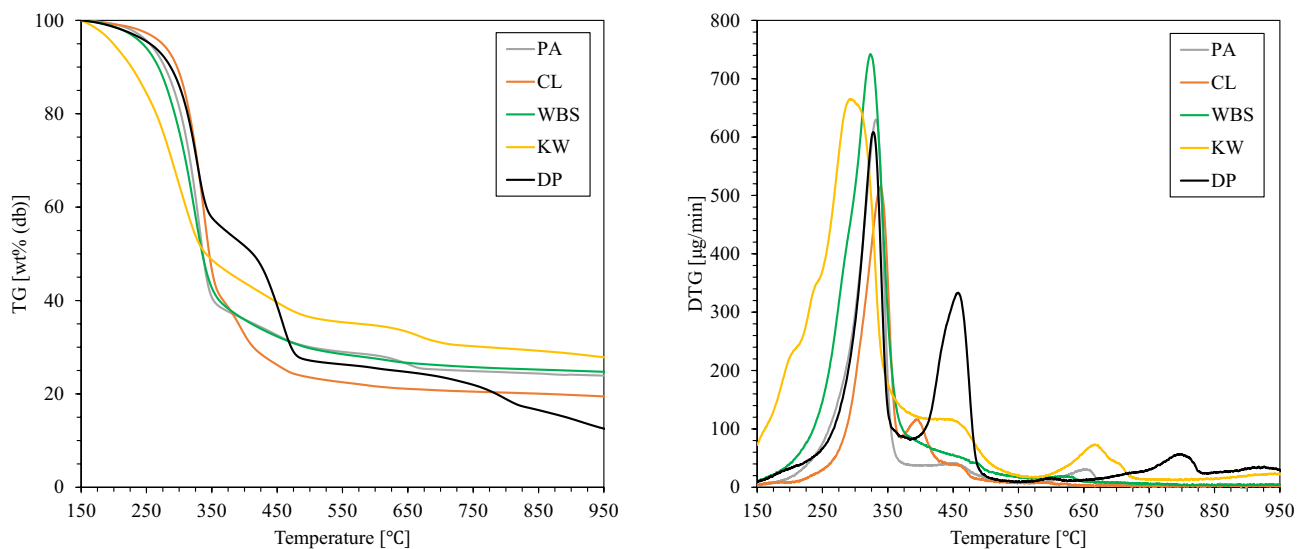


Fig. 2 Thermogravimetric (TG) and thermogravimetric derivative (DTG) curves of biomass (N_2 , $10\text{ }^\circ\text{C}/\text{min}$)

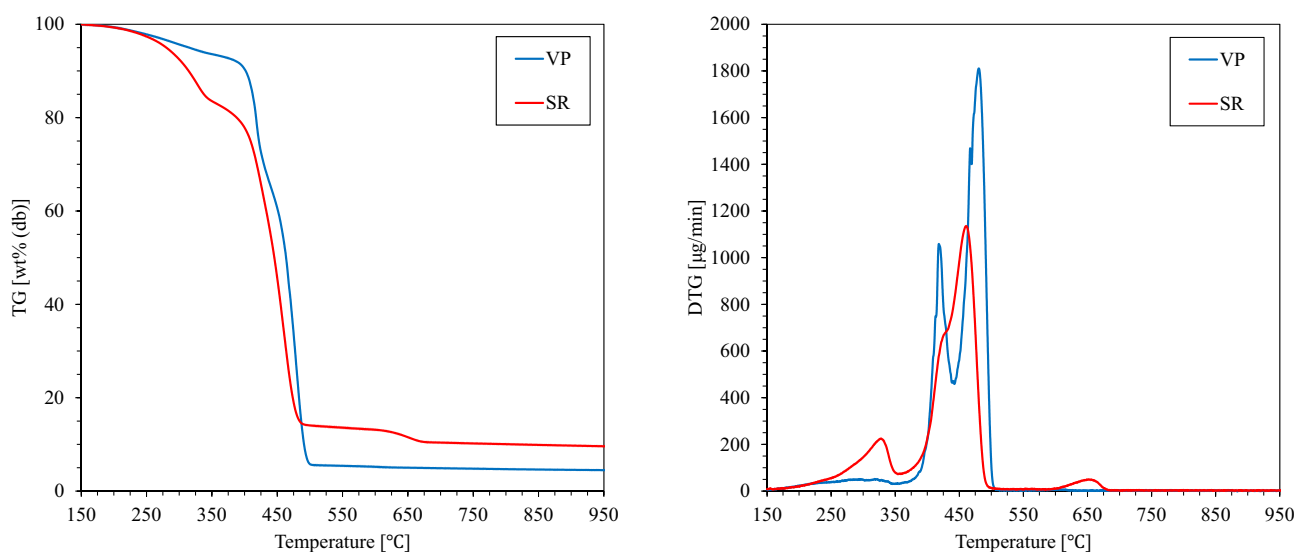


Fig. 3 Thermogravimetric (TG) and thermogravimetric derivative (DTG) curves of plastic (N_2 , $10\text{ }^\circ\text{C}/\text{min}$)

was categorized into biomass and plastics as experimental samples. The principal pyrolysis temperature range for biomass was determined to be 291 to $331\text{ }^\circ\text{C}$. Conversely, plastics exhibited a higher pyrolysis temperature range of 418 to $480\text{ }^\circ\text{C}$, indicating an elevated temperature range compared to biomass.

Biomass exhibits multiple peaks in the thermogravimetric derivative curve for each component. Among the four components, KW demonstrated the lowest pyrolysis

temperatures, while the other four components exhibited similar trends. Notably, KW and DP displayed a distinct weight loss at $450\text{ }^\circ\text{C}$, whereas PA, KW, and DP showcased a minor weight loss above $600\text{ }^\circ\text{C}$. Typical components of biomass encompass cellulose, hemicellulose, and lignin. It is widely recognized that hemicellulose, lacking a crystalline structure, undergoes pyrolysis within the lowest temperature range of 250 to $350\text{ }^\circ\text{C}$, followed by cellulose pyrolysis at 350 to $450\text{ }^\circ\text{C}$ and, subsequently, lignin pyrolysis at 400 to

550 °C [33]. Consequently, in the biomass used in this study, the pyrolysis behavior at low temperatures may be ascribed to hemicellulose, cellulose, or structurally similar sugars, while the pyrolysis behavior at higher temperatures likely arises from thermally stable structures like lignin.

In contrast, plastics primarily undergo pyrolysis reactions within the temperature range of 400 to 500 °C, with SR exhibiting a minor weight loss at a low temperature of 327 °C. The pyrolysis temperature ranges for polyethylene, polypropylene, and polystyrene, which are representative plastics, are reported to be approximately 350 to 500 °C [35, 36], respectively. Remarkably, for the plastics used in this study, the major pyrolysis temperature ranges align with those obtained for individual plastic components.

Pyrolysis and gasification experiment with MSW

Product yields

Figure 4 shows the product yield obtained from the pyrolysis and gasification of MSW (biomass and plastics). In this study, the pyrolysis products were divided into six types and quantitatively assessed in accordance with prior research. Product yields were defined as the weight of each product per unit dry weight of the sample used in the experiment. A comparison of the char quantities generated reveals 0.26 to 0.33 g/g–sample (db) for biomass and 0.04 g/g–sample (db) for plastics. Notably, plastics experience substantial volatilization above the pyrolysis temperature. The trend of char observed in biomass demonstrates a reduction in the amount

of char produced as the heating temperature increases. The experimental methodology employed herein entails an escalation in the heating rate with increasing temperature. The maximum heating rates observed near the sample when the biomass was heated were 1.54, 3.31 and 5.06 °C/s at 450, 550 and 650 °C, respectively. As a result, the pyrolysis temperature is shifted towards higher temperatures, thereby suppressing the formation of cross-links in the char structure.

During pyrolysis gasification, it is well documented that volatile matter released from pyrolysis in the solid phase undergoes repolymerization in the gas phase, followed by condensation at reduced temperatures, generating solid products such as coke and wax at room temperature and pressure. Coke is produced in minute quantities, less than 0.01 g/g–sample (db), whereas wax accounts for a relatively large proportion of the pyrolysis gasification products of plastics, ranging from 0.06 to 0.16 g/g–sample (db). Notably, it does not exhibit a discernible suppression or reduction with increasing temperature, whereas wax production experiences a considerable decline. Based on these observations, we infer that the presence of coke in the biomass identified in this study can be attributed to the growth of polycyclic aromatic hydrocarbons (PAHs), a well-known pathway for coke formation. Conversely, waxes represent aliphatic hydrocarbons of relatively high molecular weight that originate directly from plastics. Although they are produced in substantial quantities, their thermal stability is considered low. Understanding the reaction mechanism underlying the formation of these recompensates is of paramount importance, as it may serve as the main reaction pathway to pipe blockage, a prevalent issue encountered in pyrolysis gasification, and is intricately linked to tar formation.

Tar composition

Figures 5 and 6 present representative examples of the qualitative composition of biomass and plastic tar using GC/MS. The results are shown here for pyrolysis and gasification at an S/C ratio of 2 and a temperature of 550 °C. Tables 4 and 5 list the components. This table shows the relative percentage of Area values as a reference for concentrations. In this study, a concentration method by evaporation utilizing the difference in boiling points was used to separate acetone and IPA solvents from the tar, enabling accurate quantification of tar components with relatively high boiling points. It should be noted, however, that some low-boiling components may volatilize during this process. Therefore, in order to qualify components with low boiling points, qualitative analysis by GC/MS was performed on solutions before and after the tar enrichment process. Figures 5 and 6 demonstrate the compositional changes during the enrichment process, with tar, possessing a relatively high boiling point, emerging as the main component after enrichment.

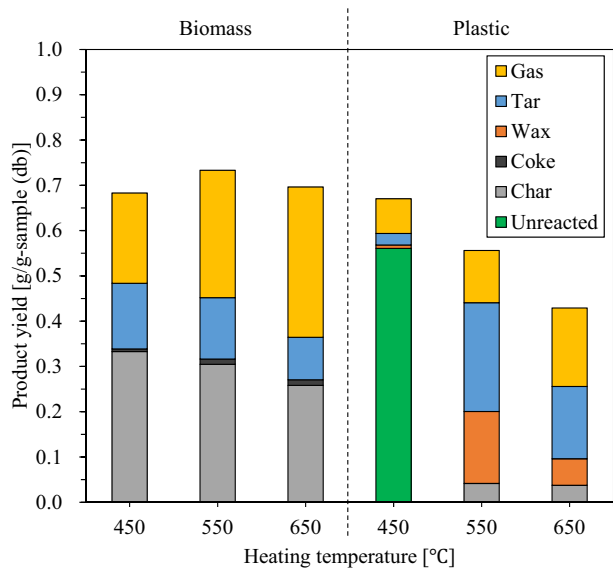


Fig. 4 Product yield in pyrolysis and gasification of MSW (biomass and plastic)

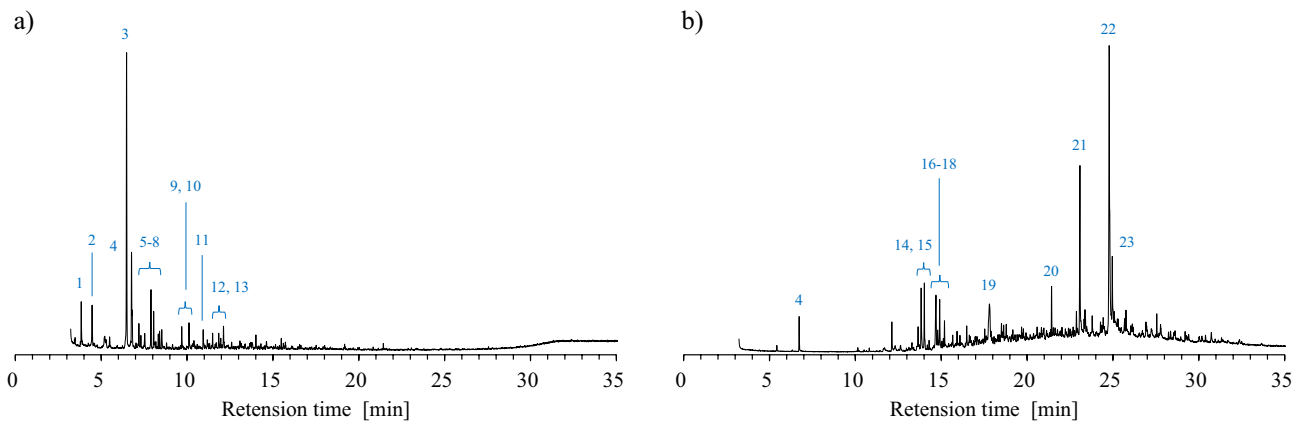


Fig. 5 GC/MS chromatograms of tar in pyrolysis and gasification of biomass ($N_2 + H_2O$, S/C=2, 550 °C). **a** Before enrichment treatment; **b** after enrichment treatment. Corresponding to Table 4

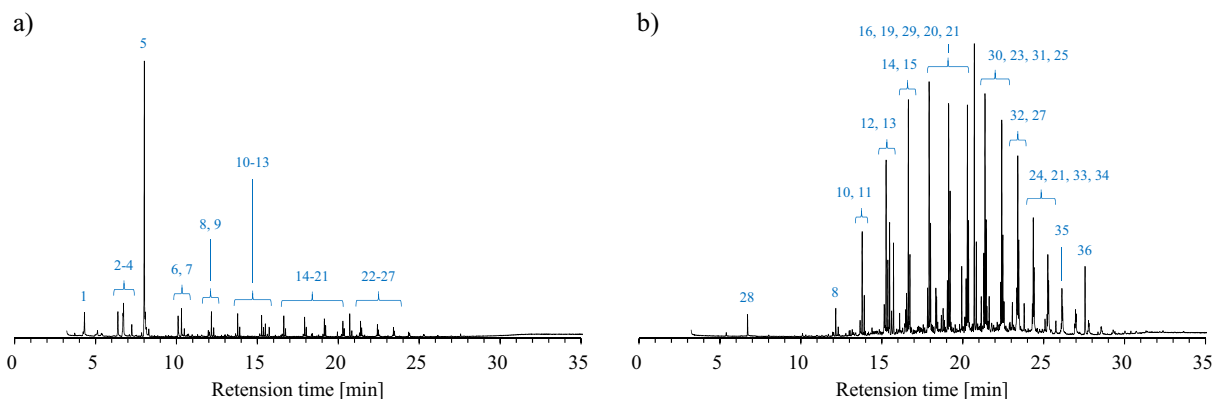


Fig. 6 GC/MS chromatograms of tar in pyrolysis and gasification of plastic ($N_2 + H_2O$, S/C=2, 550 °C). **a** Before enrichment treatment; **b** after enrichment treatment. Corresponding to Table 5

Regarding biomass tar components, the presence of oxygen-containing components, including acids, alcohols, and phenols, commonly reported in pyrolysis at low temperatures, was observed. Additionally, anhydrosugars (levoglucosan), which may be ascribed to the structure of cellulose, hemicellulose, and other sugars, were also detected. MSW tar was characterized by a high ratio of saturated fatty acids such as stearic acid and palmitic acid, and low levels of phenols derived mainly from lignin, which are often observed in the low-temperature pyrolysis of wood and other materials. These characteristics are different from those of tar components produced by pyrolysis and gasification of simply vegetable feedstocks only and may be due to the coexistence of animal-derived feedstocks such as some CL, KW, and DP. On the other hand, the formation of PAHs, such as naphthalene, frequently reported as a tar component, was minimal. This absence of PAHs is likely a result of pyrolysis and gasification occurring at temperatures below 700 °C. Comparing the composition

of the components before and after enrichment, a significant loss was observed for components with boiling points below 250 °C.

In contrast, in the case of plastics, aliphatic hydrocarbons with varying molecular weights were randomly formed. The detected aliphatic hydrocarbons mainly consisted of those with carbon chain lengths of 10 or more, many of which exhibited high boiling points compared to the tar components of the biomass. These aliphatic hydrocarbons likely stem from plastic components with a simplified chain structure, such as polyethylene and polypropylene. Additionally, they may exist in a high-molecular-weight state within the volatiles released to the gas phase after initial pyrolysis in the solid phase. In the context of plastics, secondary pyrolysis in the gas phase is considered to exert a great impact on the final product, necessitating a detailed investigation into the thermal stability and reforming behavior of the volatilized tar components.

Table 4 Tar components in pyrolysis and gasification of biomass ($N_2 + H_2O$, $S/C = 2$, $550\text{ }^\circ\text{C}$).

No	Compounds	Formula	MW	(a) [Area%]	(b) [Area%]
Oxygen-containing compounds					
1	Propylene Glycol	$C_3H_8O_2$	76.09	5.48	–
3	2,2'-(Ethylenebis(oxy))bispropane	$C_8H_{18}O_2$	146.22	45.98	–
4	4-Hydroxy-4-methyl-2-pentanone	$C_6H_{12}O_2$	116.16	17.80	2.78
5	3-Furanmethanol	$C_5H_6O_2$	98.10	2.62	–
8	2-Methyl-2-cyclopenten-1-one	C_6H_8O	96.12	2.07	–
10	Phenol	C_6H_6O	94.11	3.08	–
11	3-Methyl-1,2-cyclopentanedione	$C_6H_8O_2$	112.12	3.38	–
12	2-Methyl-phenol	C_7H_8O	108.13	1.68	–
13	4-Methyl-phenol	$C_5H_6O_2$	108.13	2.27	–
14	1,2-Benzenediol	$C_6H_6O_2$	110.11	–	5.73
15	1,4:3,6-Dianhydro- α -d-glucopyranose	$C_6H_8O_4$	144.12	–	5.41
16	Caprolactam	$C_6H_{11}NO$	113.16	–	6.53
17	Hydroquinone	$C_6H_6O_2$	110.11	–	4.23
18	4-Methyl-1,2-benzenediol	$C_7H_8O_2$	124.13	–	1.69
19	1,6-Anhydro- β -d-glucopyranose	$C_6H_{10}O_5$	162.14	–	9.11
21	n-Hexadecenoic acid	$C_{16}H_{32}O_2$	256.42	–	14.45
22	(Z)-6-Octadecenoic acid	$C_{18}H_{34}O_2$	282.45	–	41.07
23	Octadecanoic acid	$C_{18}H_{36}O_2$	284.47	–	5.53
Aromatic compounds					
2	Toluene	C_7H_8	92.13	6.93	–
6	Ethylbenzene	C_8H_{10}	106.16	1.58	–
7	Styrene	C_8H_8	104.14	4.18	–
20	Anthracene	$C_{14}H_{10}$	178.22	–	3.46
Aliphatic hydrocarbons					
9	3-Methyl-1-butyne	C_5H_8	68.11	2.94	–

(a) before enrichment treatment; (b) after enrichment treatment. Corresponding to Fig. 5

Gas composition

Figure 7 illustrates the production of the four primary gas components (H_2 , CH_4 , CO , and CO_2) along with the cumulative sum of other lower hydrocarbons (C_xH_y), resulting in a total of five components at various heating temperatures. The quantities of lower hydrocarbon components (C_2H_2 , C_2H_4 , C_2H_6 , C_3H_6 , C_3H_8 , butane, and isobutane) generated are presented in Fig. 8.

In biomass, CO_2 emerges as the most abundant component at all temperatures, followed by H_2 , CO , and CH_4 . The formation of low-grade hydrocarbons occurs in trace amounts relative to inorganic gases. Typically, during the pyrolysis of cellulose and hemicellulose, the sequential cleavage of glycosidic bonds and the ring-opening of cyclic sugars progress at $200\text{ }^\circ\text{C}$ – $300\text{ }^\circ\text{C}$, concomitant with simultaneous decarboxylation reactions that result in remarkable CO_2 release during the initial stage of pyrolysis [36]. In our study, a high percentage of CO_2 was produced at $450\text{ }^\circ\text{C}$, which is considered to originate from the decarboxylation reaction in the early pyrolysis phase. Notably, there was a pronounced increase in gas production with increasing

temperatures. Gasification and reforming reactions of char and tar involving steam do not have sufficient reaction rates in the temperature range below $700\text{ }^\circ\text{C}$ [37]. Conversely, alkali and alkaline acid-alkaline metals (AAEMs) present in biomass are recognized catalysts in gasification reactions [38], suggesting their potential contribution to the rise in H_2 and CO_2 levels within biomass between 450 and $650\text{ }^\circ\text{C}$.

Plastics had lower total gas production than that of biomass at temperatures below $650\text{ }^\circ\text{C}$. The elemental composition of plastics, characterized by reduced oxygen content, led to relatively modest CO and CO_2 production. Consequently, there was a more pronounced occurrence of lower hydrocarbon generation relative to inorganic gases. The production of lower hydrocarbons increased markedly with increasing temperatures, especially at $650\text{ }^\circ\text{C}$. In plastics, aliphatic hydrocarbons released into the gas phase after pyrolysis are successively reduced to gas, necessitating heating temperatures above $650\text{ }^\circ\text{C}$ and extended residence times to facilitate sufficient decomposition. Conversely, CO_2 and H_2 in plastics demonstrated minimal fluctuations within the temperature range of $450\text{ }^\circ\text{C}$ – $650\text{ }^\circ\text{C}$, implying the absence of steam gasification. Considering the scarcity of AAEMs in plastics, this

Table 5 Tar components in pyrolysis and gasification of plastic (N₂ + H₂O, S/C = 2, 550 °C).

No	Compounds	Formula	MW	(a) [Area%]	(b) [Area%]
Oxygen-containing compounds					
2	2,2'-(Ethylenebis(oxy))bispropane	C ₈ H ₁₈ O ₂	146.22	4.72	–
28	4-Hydroxy-4-methyl-2-pentanone	C ₆ H ₁₂ O ₂	116.16	–	0.89
29	E-15-Heptadecenal	C ₁₇ H ₃₂ O	252.43	–	–
Aromatic compounds					
1	Toluene	C ₇ H ₈	92.13	3.74	–
4	Ethylbenzene	C ₈ H ₁₀	106.16	1.97	–
5	Styrene	C ₈ H ₈	104.14	46.77	–
6	α-Methylstyrene	C ₉ H ₁₀	118.17	2.47	–
30	1,3-Diphenylpropane	C ₁₅ H ₁₆	196.28	–	2.21
Aliphatic hydrocarbons					
3	2,4-Dimethyl-1-heptene	C ₉ H ₁₈	140.26	5.68	–
7	1-Decene	C ₁₀ H ₂₀	154.29	3.68	–
8	1-Undecene	C ₁₁ H ₂₂	156.30	3.41	0.28
9	Undecane	C ₁₁ H ₂₄	168.31	1.11	–
10	1-Dodecene	C ₁₂ H ₂₄	170.33	2.72	3.37
11	Dodecane	C ₁₂ H ₂₆	140.26	1.14	1.35
12	1-Tridecene	C ₁₃ H ₂₆	182.34	2.31	5.28
13	Tridecane	C ₁₃ H ₂₈	184.35	1.42	3.56
14	1-Tetradecene	C ₁₄ H ₂₈	196.36	2.45	7.16
15	Tetradecane	C ₁₄ H ₃₀	198.38	0.89	2.38
16	1-Pentadecene	C ₁₅ H ₃₀	210.39	2.20	7.47
17	Pentadecane	C ₁₅ H ₃₂	212.41	0.91	3.49
18	1-Hexadecene	C ₁₆ H ₃₂	224.42	1.92	7.11
19	Hexadecane	C ₁₆ H ₃₄	226.43	1.19	4.22
20	(Z)-3-Heptadecene	C ₁₇ H ₃₄	238.44	1.74	6.74
21	Heptadecane	C ₁₇ H ₃₆	240.46	0.88	5.57
22	1-Octadecene	C ₁₈ H ₃₆	252.47	1.81	6.87
23	Octadecane	C ₁₈ H ₃₈	254.48	0.85	3.34
24	1-Nonadecene	C ₁₉ H ₃₈	266.49	1.46	3.45
25	Nonadecane	C ₁₉ H ₄₀	268.51	0.71	2.81
26	1-Eicosene	C ₂₀ H ₄₀	280.52	0.98	–
27	Eicosane	C ₂₀ H ₄₂	282.54	0.88	3.71
31	Z-5-Nonadecene	C ₁₉ H ₃₈	266.49	–	6.07
32	(E)-5-Eicosene	C ₂₀ H ₄₀	280.52	–	4.60
33	1-Docosene	C ₂₂ H ₄₄	308.57	–	2.13
34	Docosane	C ₂₂ H ₄₆	310.59	–	2.09
35	11-Tricosene	C ₂₃ H ₄₆	322.60	–	1.20
36	(E)-3-Eicosene	C ₂₀ H ₄₀	280.52	–	2.66

(a) before enrichment treatment; (b) after enrichment treatment. Corresponding to Fig. 6

observation supports the notion that AAEMs present in biomass effectively act as catalysts in steam reaction processes.

In the pyrolysis gasification process, the formation of tar and soot from the growth of PAHs poses a recurring challenge due to its propensity for pipe blockages. The reaction mechanism involving acetylene (C₂H₂) and ethylene (C₂H₄) is recognized as playing a crucial role in the formation pathway of PAHs. Pyrolysis and gasification of

MSW, which compete with the production of lower hydrocarbons from plastics with the reaction of biomass that produces many monocyclic aromatic compounds due to the pyrolysis of lignin, may promote the growth of PAHs in secondary gas-phase reactions, and the gas composition at 450–650 °C in this study is important to estimate the precursors of these secondary reactions.

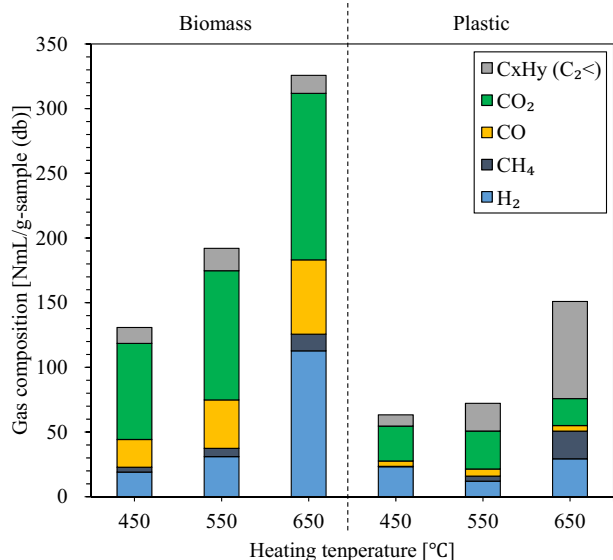


Fig. 7 Production of major gas components (H_2 , CH_4 , CO , CO_2 , and C_xH_y) in pyrolysis and gasification of MSW (biomass and plastic)

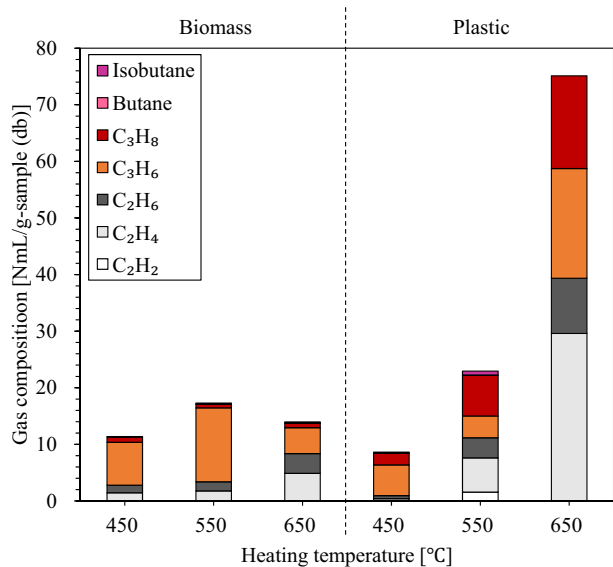


Fig. 8 Production of lower hydrocarbons (C_2H_2 , C_2H_4 , C_2H_6 , C_3H_6 , C_3H_8 , butane, and isobutane) in pyrolysis and gasification of MSW (biomass and plastic)

Heat of reaction in the pyrolysis and gasification of MSW

In this study, the heat balance in the reaction process was assessed by measuring the HHV of the products. The heat of reaction was determined using Eq. (1), following the established thermodynamic conventions [39].

$$Q_r = \sum HHV_{Product} - \sum HHV_{Reactant} \quad (1)$$

where Q_r represents the heat of reaction, $HHV_{Product}$ denotes the higher heating value of the product, and $HHV_{Reactant}$ corresponds to the higher heating value of the reactant.

Table 6 displays the HHV of each product used in the calculations. For products where obtaining the required sample volume for HHV proved challenging, several assumptions were made, which are enumerated below. In the case of coke, naphthalene was assumed as the representative component [40], and HHV of 43,320 J/g (db) was calculated using the standard enthalpy of formation of naphthalene (150.3 kJ/mol) at 279.15 K. As previously described, low-boiling-point tar is lost during the tar enrichment process. The components present in the lost tar from biomass were defined as those with a boiling point of 200 °C or lower, based on the findings of the qualitative analysis outlined in Sect. "Tar composition". The HHV of the lost tar was calculated based on the literature values of tar components [41]. Regarding the lost tar from plastics, n-decane was assumed as the representative component, and its higher heating value was calculated. The amount of lost tar was determined based on the carbon yield of the product. The lost carbon was 22.61, 17.99, and 27.99 wt% at 450, 550, and 650 °C for the biomass, based on total carbon in the feedstock. Under the present assumptions, the lost tar yields at 450, 550, and 650 °C were estimated from the carbon yields to be 0.18, 0.15, and 0.23 g/g-sample (db), respectively. Similarly, for plastics, the carbon loss was 37.91, 51.79 and 62.44 wt% at 450, 550 and 650 °C, and the lost tar yield was estimated to be 0.20, 0.28 and 0.34 g/g-sample (db), respectively. As for the gases, the HHV of the product gases under each condition were obtained using Eq. (2) using the qualitative and quantitative analysis values from Sect. "Gas composition".

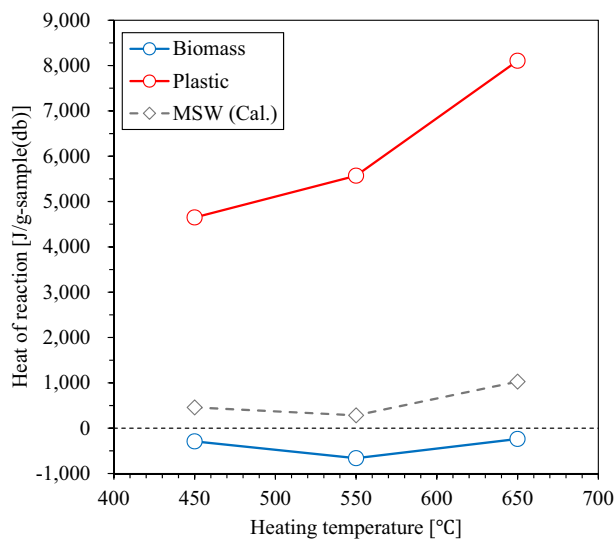
$$HHV_{Gas} = \frac{\sum (HHV_i \times M_i)}{M_{Gas}} \quad (2)$$

where HHV_{Gas} represents the HHV of the product gas, HHV_i signifies the HHV of each gas component, M_{Gas} denotes the weight of the product gas, and M_i corresponds to the weight of each gas component. Other missing calculated values were determined following the procedures outlined in the notes of Table 6.

The calculated heat of reaction is shown in Fig. 9. Figure 9 illustrates the results for biomass (denoted by the blue line) and plastics (denoted by the red line). Additionally, the calculations for waste (denoted by the gray dotted line) are included, where the results of each component are multiplied by their respective existence ratio (as provided in Table 1) and collated. In the case of biomass, the reactions were slightly exothermic, with values ranging from -661 to -237 J/g-sample (db). Plastics exhibited highly endothermic reactions, ranging from 4649 to 8106 J/g-sample (db). In

Table 6 HHV of products in pyrolysis and gasification of MSW (biomass and plastic)

	Biomass			Plastic		
	HHV [J/g (db)]					
	450 °C	550 °C	650 °C	450 °C	550 °C	650 °C
Unreacted	–	–	–	44,268	–	–
Char	20,160	19,450	18,500	–	9,000 ²	9,000 ²
Coke	43,320 ¹	43,320 ¹	43,320 ¹	–	–	–
Wax	–	–	–	–	45,190	43,990
Tar	26,440	30,140	28,670	42,640 ³	42,640	42,310
Loss tar ¹	26,640 ¹	26,640 ¹	26,640 ¹	54,252 ¹	54,252 ¹	54,252 ¹
Gas	8,717	9,391	10,290	14,971	18,383	36,295

¹Calculated value²The HHV of plastic char were measured by mixing char sampled at 550 and 650 °C³Due to insufficient sampling, the measured value of 550 °C was used for the calculation**Fig. 9** Heat of reaction in pyrolysis and gasification of MSW (biomass and plastic)

biomass, exothermic reactions involving the formation of intermolecular cross-links through carbonization compete with the endothermic reactions of product decomposition and secondary reactions. It is widely recognized that in the low-temperature range, the heat of reaction approaches a value close to zero [26, 39]. The heat of reaction of the biomass tended to shift slightly toward the exothermic side between 450 and 550 °C and again toward the exothermic side between 550 and 650 °C. The heat retained by the product at each heating temperature is dominated by char at lower temperatures and by gas at higher temperatures. Therefore, a more detailed study is needed to discuss small differences in the reaction heat of biomass, since the balanced intermediate temperature depends on the accuracy of the estimation of the

lost tar heat. In contrast, the pyrolysis process for plastics requires significantly higher reaction heat than the pyrolysis process for biomass because it involves only minimal carbonization and is dominated by endothermic reactions. In the overarching context of the pyrolysis and gasification mechanisms applied to plastics, an escalation in the plastic's temperature prompts a competition between volatilization, arising from decomposition occurring at the terminal junctures within the polymer chain, and pyrolysis in the liquid phase stemming from the act of melting. Consequently, the resultant pyrolysis products achieving their boiling point in the liquid phase undergo release into the gaseous phase. Numerous volatile compounds exhibit a lack of thermal stability and undergo sequential secondary degradation due to the mixture of end-radicalized fragments [42]. Specifically, it has been reported that the polystyrene, which produces monomers with low boiling points in the early stages of the reaction, can markedly alter the product composition through the regulation of secondary reactions [43]. Considering these factors, it can be inferred that the endothermic reaction of plastics is influenced by the gas-phase reaction to a certain extent. In addition, char gasification and tar reforming reactions with steam, which mainly involve the formation of hydrogen, are large endothermic reactions. Considering that the heat of reaction for the biomass in this study was near zero and that the hydrogen production from the plastics was low, the effect of the steam-related reactions on the estimated heat of reaction is considered to be small.

Furthermore, Table 6 shows that the heat retained by the tar and gas of plastic origin is very high in the pyrolysis and gasification products of MSW. For the purpose of energy recovery from MSW, these products with high heat retention need to be controlled. While previous studies have focused extensively on mass balance in pyrolysis and gasification products, limited attention has been given to heat balance. Therefore, the calculated reaction heat value in this study

serves as an indicator for addressing the pyrolysis gasification of MSW. Further exploration and experimental and numerical analysis of the thermal aspects of pyrolysis and gasification reactions in gasifiers will contribute to the development of more advanced designs.

Conclusions

Experimental investigations on pyrolysis and gasification experiments were conducted using actual MSW samples obtained from an operational MSW incineration plant. The study yielded significant findings regarding the pyrolysis and gasification characteristics of MSW, encompassing both biomass and plastic components. The key conclusions are as follows:

- 1) Among the MSW components, the main pyrolysis temperature range for biomass is approximately 291 to 331 °C, whereas for plastics, it ranges from 418 to 480 °C. The reaction in biomass occurred across multiple temperature ranges, whereas for plastics, a single reaction dominated.
- 2) In terms of the fundamental MSW pyrolysis and gasification products, it was inferred that char primarily originated from biomass, while tar and wax in the volatile matter were mainly derived from plastics.
- 3) The tar components of biomass exhibited the distinct characteristic of containing oxygenated hydrocarbons, often structured in ring formations. In contrast, aliphatic hydrocarbons were abundant in the plastics, and the properties of the tar components differed greatly.
- 4) In the case of biomass, hydrogen and carbon dioxide were the primary constituents of the produced gas, whereas lower hydrocarbons were the main components in the case of plastics.
- 5) The HHV of the products were measured, and the heat balance was investigated. The determined reaction heats ranged from -661 to -237 J/g-sample (db) (exothermic reaction) for biomass and from 4649 to 8106 J/g-sample (db) (endothermic reaction) for plastics under the specific pyrolysis and gasification conditions in this study.

References

1. In: Meti.go.jp. https://www.enecho.meti.go.jp/category/others/basic_plan/pdf/strategic_energy_plan.pdf. Accessed 18 Apr 2023
2. In: Env.go.jp. <https://www.env.go.jp/policy/hakusyo/r04/pdf/full.pdf>. Accessed 18 Apr 2023
3. In: Env.go.jp. <https://www.env.go.jp/content/900534340.pdf>. Accessed 18 Apr 2023
4. In: Env.go.jp. https://www.env.go.jp/recycle/waste_tech/ippan/r2/data/disposal.pdf. Accessed 18 Apr 2023
5. Chen D, Yin L, Wang H, He P (2015) Reprint of: Pyrolysis technologies for municipal solid waste: a review. *Waste Manag* 37:116–136. <https://doi.org/10.1016/j.wasman.2015.01.022>
6. Franco C, Pinto F, Gulyurtlu I, Cabrita I (2003) The study of reactions influencing the biomass steam gasification process☆. *Fuel (Lond)* 82:835–842. [https://doi.org/10.1016/s0016-2361\(02\)00313-7](https://doi.org/10.1016/s0016-2361(02)00313-7)
7. Kobayashi J, Kawamoto K, Fukushima R, Tanaka S (2011) Woody biomass and RPF gasification using reforming catalyst and calcium oxide. *Chemosphere* 83:1273–1278. <https://doi.org/10.1016/j.chemosphere.2011.03.010>
8. In: Nedo.go.jp. <https://www.nedo.go.jp/content/100544819.pdf>. Accessed 18 Apr 2023
9. Arena U (2012) Process and technological aspects of municipal solid waste gasification. A review. *Waste Manag* 32:625–639. <https://doi.org/10.1016/j.wasman.2011.09.025>
10. Buah WK, Cunliffe AM, Williams PT (2007) Characterization of products from the pyrolysis of municipal solid waste. *Process Saf Environ Prot* 85:450–457. <https://doi.org/10.1205/psep07024>
11. Luo S, Xiao B, Hu Z, Liu S, Guan Y, Cai L (2010) Influence of particle size on pyrolysis and gasification performance of municipal solid waste in a fixed bed reactor. *Bioresour Technol* 101:6517–6520. <https://doi.org/10.1016/j.biortech.2010.03.060>
12. Bhoi PR, Huhnke RL, Kumar A, Indrawan N, Thapa S (2018) Co-gasification of municipal solid waste and biomass in a commercial scale downdraft gasifier. *Energy* 163:513–518. <https://doi.org/10.1016/j.energy.2018.08.151>
13. Cerone N, Zimbardi F, Contuzzi L, Baleta J, Cerinski D, Skvorčinskienė R (2020) Experimental investigation of syngas composition variation along updraft fixed bed gasifier. *Energy Convers Manag* 221:113116. <https://doi.org/10.1016/j.enconman.2020.113116>
14. Arena U, Zaccariello L, Mastellone ML (2010) Fluidized bed gasification of waste-derived fuels. *Waste Manag* 30:1212–1219. <https://doi.org/10.1016/j.wasman.2010.01.038>
15. Win MM, Asari M, Hayakawa R, Hosoda H, Yano J, Sakai S (2019) Characteristics of gas from the fluidized bed gasification of refuse paper and plastic fuel (RPF) and wood biomass. *Waste Manag* 87:173–182. <https://doi.org/10.1016/j.wasman.2019.02.002>
16. Fantozzi F, Colantoni S, Bartocci P, Desideri U (2007) Rotary kiln slow pyrolysis for syngas and char production from biomass and waste—part I: Working envelope of the reactor. *J Eng Gas Turbine Power* 129:901–907. <https://doi.org/10.1115/1.2720521>
17. Fantozzi F, Colantoni S, Bartocci P, Desideri U (2007) Rotary kiln slow pyrolysis for syngas and char production from biomass and waste — part II: Introducing product yields in the energy balance. *J Eng Gas Turbine Power* 129:908–913. <https://doi.org/10.1115/1.2720539>
18. Molino A, Iovane P, Donatelli A, Baraccio G, Chianese S, Musmarra D (2013). Steam gasification of refuse-derived fuel in a rotary kiln pilot plant: Experimental tests. <https://doi.org/10.3303/CET1332057>. Accessed 14 Jun 2023
19. Li S-Q, Yan J-H, Li R-D, Chi Y, Cen K-F (2002) Axial transport and residence time of MSW in rotary kilns. *Powder Technol* 126:217–227. [https://doi.org/10.1016/s0032-5910\(02\)00014-1](https://doi.org/10.1016/s0032-5910(02)00014-1)
20. Hasan MM, Rasul MG, Khan MMK, Ashwath N, Jahirul MI (2021) Energy recovery from municipal solid waste using pyrolysis technology: a review on current status and developments. *Renew Sustain Energy Rev* 145:111073. <https://doi.org/10.1016/j.rser.2021.111073>
21. Kern S, Halwachs M, Kampichler G, Pfeifer C, Pröll T, Hofbauer H (2012) Rotary kiln pyrolysis of straw and fermentation residues in a 3MW pilot plant – Influence of pyrolysis temperature on

- pyrolysis product performance. *J Anal Appl Pyrolysis* 97:1–10. <https://doi.org/10.1016/j.jaap.2012.05.006>
22. Asmadi M, Kawamoto H, Saka S (2017) Characteristics of softwood and hardwood pyrolysis in an ampoule reactor. *J Anal Appl Pyrolysis* 124:523–535. <https://doi.org/10.1016/j.jaap.2017.01.029>
 23. Duong TL, Nguyen DT, Nguyen HHM, Phan BMQ, Nguyen HL, Huynh TM (2019) Fast pyrolysis of Vietnamese waste biomass: relationship between biomass composition, reaction conditions, and pyrolysis products, and a strategy to use a biomass mixture as feedstock for bio-oil production. *J Mater Cycles Waste Manag* 21:624–632. <https://doi.org/10.1007/s10163-018-00823-z>
 24. Win MM, Asari M, Hayakawa R, Hosoda H, Yano J, Sakai S (2020) Gas and tar generation behavior during flash pyrolysis of wood pellet and plastic. *J Mater Cycles Waste Manag* 22:547–555. <https://doi.org/10.1007/s10163-019-00949-8>
 25. Hwang I-H, Kobayashi J, Kawamoto K (2014) Characterization of products obtained from pyrolysis and steam gasification of wood waste, RDF, and RPF. *Waste Manag* 34:402–410. <https://doi.org/10.1016/j.wasman.2013.10.009>
 26. Rath J, Wolfinger MG, Steiner G, Krammer G, Barontini F, Cozzani V (2003) Heat of wood pyrolysis. *Fuel* 82:81–91. [https://doi.org/10.1016/S0016-2361\(02\)00138-2](https://doi.org/10.1016/S0016-2361(02)00138-2)
 27. Ansah E, Wang L, Shahbazi A (2016) Thermogravimetric and calorimetric characteristics during co-pyrolysis of municipal solid waste components. *Waste Manag* 56:196–206. <https://doi.org/10.1016/j.wasman.2016.06.015>
 28. Straka P, Bičáková O, Šupová M (2017) Thermal conversion of polyolefins/polystyrene ternary mixtures: kinetics and pyrolysis on a laboratory and commercial scales. *J Anal Appl Pyrolysis* 128:196–207. <https://doi.org/10.1016/j.jaap.2017.10.010>
 29. In: Env.go.jp. <http://www.env.go.jp/hourei/11/000013.html>. Accessed 18 Apr 2023
 30. Matsuto T, Ishii S (2011) Proximate and ultimate analysis for detailed composition of combustible fractions in household waste. *J Jpn Soc Mater Cycles Waste Manag* 22:382–395. <https://doi.org/10.3985/jjmscwm.22.382>
 31. Himeno S, Iyatomi Y, Komatsu T, Fujita S (2004) Modeling of municipal solid waste (MSW) pyrolysis reaction by thermal analysis. *J Jpn Soc Waste Manag Experts* 15:105–113. <https://doi.org/10.3985/jswme.15.105>
 32. Zheng J, Jin Y-Q, Chi Y, Wen J, Jiang X, Ni M (2009) Pyrolysis characteristics of organic components of municipal solid waste at high heating rates. *Waste Manag* 29:1089–1094. <https://doi.org/10.1016/j.wasman.2008.06.034>
 33. Cortazar M, Santamaria L, Lopez G, Alvarez J, Zhang L, Wang R, Bi X, Olazar M (2023) A comprehensive review of primary strategies for tar removal in biomass gasification. *Energy Convers Manag* 276:116496. <https://doi.org/10.1016/j.enconman.2022.116496>
 34. Hosoya T, Kawamoto H, Saka S (2008) Different pyrolytic pathways of levoglucosan in vapor- and liquid/solid-phases. *J Anal Appl Pyrolysis* 83:64–70. <https://doi.org/10.1016/j.jaap.2008.06.008>
 35. JIS M 8814:2003 Coal and coke-Determination of gross calorific value by the bomb calorimetric method, and calculation of net calorific value
 36. Shen DK, Gu S, Bridgwater AV (2010) Study on the pyrolytic behaviour of xylan-based hemicellulose using TG–FTIR and Py–GC–FTIR. *J Anal Appl Pyrolysis* 87:199–206. <https://doi.org/10.1016/j.jaap.2009.12.001>
 37. Franco C, Pinto F, Gulyurtlu I, Cabrita I (2003) The study of reactions influencing the biomass steam gasification process ☆. *Fuel* 82:835–842. [https://doi.org/10.1016/S0016-2361\(02\)00313-7](https://doi.org/10.1016/S0016-2361(02)00313-7)
 38. Yu J, Guo Q, Gong Y, Ding L, Wang J, Yu G (2021) A review of the effects of alkali and alkaline earth metal species on biomass gasification. *Fuel Process Technol* 214:106723. <https://doi.org/10.1016/j.fuproc.2021.106723>
 39. Kodera Y, Kaiho M (2016) Model calculation of heat balance of wood pyrolysis. *J Jpn Inst Energy* 95:881–889. <https://doi.org/10.3775/jie.95.881>
 40. He Q, Guo Q, Umeki K, Ding Lu, Wang F, Yu G (2021) Soot formation during biomass gasification: a critical review. *Renew Sustain Energy Rev* 139:110710. <https://doi.org/10.1016/j.rser.2021.110710>
 41. Zhang Y, Kajitani S, Ashizawa M, Oki Y (2010) Tar destruction and coke formation during rapid pyrolysis and gasification of biomass in a drop-tube furnace. *Fuel* 89:302–309. <https://doi.org/10.1016/j.fuel.2009.08.045>
 42. Hernández M, García Á, Gómez A, Agulló J, Marcilla A (2006) Effect of residence time on volatile products obtained in the HDPE pyrolysis in the presence and absence of HZSM-5. *Ind Eng Chem Res* 45:8770–8778. <https://doi.org/10.1021/ie060728+>
 43. Singh R, Ruj B, Sadhukhan A, Gupta P (2020) Thermal degradation of waste plastics under non-sweeping atmosphere: Part 2: Effect of process temperature on product characteristics and their future applications. *J Environ Manage* 261:110112. <https://doi.org/10.1016/j.jenvman.2020.110112>

Publisher's Note Springer Nature remains neutral with regard to jurisdictional claims in published maps and institutional affiliations.

Springer Nature or its licensor (e.g. a society or other partner) holds exclusive rights to this article under a publishing agreement with the author(s) or other rightsholder(s); author self-archiving of the accepted manuscript version of this article is solely governed by the terms of such publishing agreement and applicable law.